Calibration and validation of a new elastoviscoplastic soil model

Received: 21 February 2020 | Revised: 16 October 2020 | Accepted: 26 November 2020

DOI: 10.1002/nag.3173

RESEARCH ARTICLE

WILEY

Calibration and validation of a new elastoviscoplastic soil model

Yixing Yuan[1,2] | **Andrew J. Whittle**[2]

[1] GZA GeoEnvironmental Inc., Norwood, Massachusetts

[2] Department of Civil and Environmental Engineering, Massachusetts Institute of Technology, Cambridge, Massachusetts

Correspondence
Yixing Yuan, GZA GeoEnvironmental Inc., Norwood, MA.
Email: yixing.yuan@gza.com

Abstract

This paper presents the calibration and validation for a new 3D elastoviscoplastic soil model, MIT-SR, for Resedimented Boston Blue Clay (RBBC). The calibration procedure requires selection of material constants from standard types of laboratory consolidation and undrained shear tests, and a procedure for initialization of state variables. The formulation includes two key input parameters that describe sensitivity of rate dependence, β, and creep behavior, ρ_α, for which the calibration requires data including CRS consolidation tests at a range of strain rates and drained creep tests. The calibrated MIT-SR model is benchmarked through a series of simulations of K_0-consolidated triaxial shear tests and direct simple shear tests on RBBC performed at different rates of shear strain. The calibrated model provides very good predictions of the effects of shear strain rate on key engineering properties such as undrained shear strength, strain to peak shear resistance and critical state conditions as functions of the consolidation stress history. The predictions of multistage, undrained relaxation tests are also in good agreement with unique measured behavior reported for RBBC. The comparisons provide clear evidence of the advances in predictive capabilities achieved using the proposed MIT-SR formulation compared to preexisting isotache-type models.

KEYWORDS

calibration, direct simple shear, drained creep, elastoplasticity, elastoviscoplasticity, model validation, strain-rate effects, triaxial shear, undrained relaxation

1 | INTRODUCTION

The Authors have presented the formulation of a new elastoviscoplastic model, MIT-SR, for predicting rate-dependent behavior of clay under general loading conditions.[1] The proposed MIT-SR model includes a novel evolution equation that attributes viscoplastic deformation to an internal strain rate, R_a, representing the perturbation of the clay particle assembly due to historical compression and shear. The formulation is built upon a prior 3D elastoplastic framework (MIT-S1[2,3]) and unifies the descriptions of various important aspects of clay behavior, including anisotropic stress-strain-strength properties, nonlinear small strain stiffness and strain-rate effects.

The companion paper presents the complete formulation of the proposed MIT-SR model, and illustrates its versatility in capturing a wide range of rate-dependent characteristics of clays, including strain rate effects in monotonic and cyclic shear, undrained creep and undrained relaxation.[1] The current paper describes a procedure for determining the model

TABLE 1 Index properties of Resedimented Boston Blue Clay[7] and Salt Lake City clay[20]

Index property	RBBC	SLC*
Liquid limit, w_L [%]	46.5	43.5
Plasticity index, I_p [%]	22.7	21.3
Clay fraction, CF [%]	56.0	21.0
Specific gravity, G_s	2.78	2.73
USCS classification	CL	CL

*SLC: Salt Lake City clay—used for MIT-SR parameters β_2 and β_3 (Table 2).

parameters using standard types of laboratory experiments, and validates model predictions by comparing with laboratory measurements highlighting rate-dependent material behavior.

This first part of this paper focuses on the selection of model parameters for Resedimented Boston Blue Clay (RBBC). This material (with index properties summarized in Table 1) has been systematically studied through many experimental programs at MIT with well-documented engineering properties and characteristic behavior.[4–7] The natural Boston Blue Clay is an illitic, glaciomarine low plasticity (CL) clay whose properties vary markedly with details of the stratigraphy (silt content etc.).[8,9] The resedimentation technique is used to minimize variations of natural samples, leading to well-controlled consolidation stress history and reproducible test results.[6,7,10,11] For the last two decades, the experimental data of RBBC have been thoroughly used to determine parameters of the prior elastoplastic soil models including, MIT-E3[12,13] and MIT-S1.[2,3] These efforts facilitate the calibration of MIT-SR using RBBC, as some of the MIT-SR parameters can be determined with similar calibration procedures.

We then validate the MIT-SR predictions with a set of experimental data of RBBC.[4,14–16] This dataset comprises K_0-consolidated undrained compression (CK_0UC) and extension (CK_0UE) tests at different OCRs using strain rates that span three orders of magnitude, undrained relaxation during triaxial shear, and K_0-consolidated direct simple shear (CK_0DSS) tests at different OCRs. Although these data have been widely cited in the literature, existing soil models still face great difficulties in achieving consistent predictions, as the task demands a unified representation of rate-dependent properties, anisotropic stress-strain-strength characteristics and small-strain nonlinearity. This paper uses the proposed MIT-SR formulation to represent the comprehensive observations of the rate-dependent shear behavior of RBBC. The validations also shed light on the usefulness of the proposed model in applications for complex boundary value problems.

2 | CALIBRATION FOR BOSTON BLUE CLAY

The MIT-SR model uses 17 material parameters, which can all be determined from a number of standard types of laboratory tests, while most of them can be readily determined with similar method to those used in calibrating MIT-S1 parameters.[3] Table 2 summarizes the selected parameters for RBBC and the experiments used in this calibration including

(1) K_0-consolidation in incrementally loaded (IL) or constant rate of strain (CRS) oedometer or triaxial devices for determining parameters that control volumetric behavior: normally consolidated compressibility, ρ_c; hysteretic parameters, D and r; the lateral pressure coefficient, K_{0NC}; and the ratio of small strain elastic modulus, $K/2G$.
(2) K_0-consolidated undrained compression and extension, CK_0UC and CK_0UE tests (based on the SHANSEP procedure[17]) for calibrating the parameters concerning shear behavior: small strain stiffness parameter, C_b; critical state frictional angle, ϕ'_{cs}; shape factor for the loading/reference surface, m; maximum friction angle, ϕ'_m; kinematic hardening coefficient, ψ; nonlinearity for small strain shear behavior, w_s, and the dilation constant, D_L.
(3) CRS tests performed at different strain rates[18,19] are used to determine rate-sensitivity parameter, β, and reference strain rate $\dot{\varepsilon}_{ref}$.
(4) Creep data from consolidation in triaxial tests,[7] and those from incrementally loaded (IL) consolidation in oedometer or Direct Simple Shear (DSS) devices[15] are used to determine ρ_α. Creep data at overconsolidated (OC) states (for Salt Lake City (SLC) clay)[20] are used to infer parameters, β_2 and β_3.

The details about the determination of each parameter are presented as follows:

TABLE 2 Calibrated MIT-SR parameters for RBBC

Symbols	Values	Data set used for calibration	Reference
ρ_c	0.180	LCC from K_0-consolidation in triaxial tests	7
K_{0NC}	0.49	Stress state after K_0-consolidation in triaxial tests	4
C_b	473	High quality small strain measurement of G_{sec}	5
$2G/K$	1.13	1D swelling σ'_v-σ'_h effective stress paths	4, 7
D	0.03	1D swelling log$e$-logσ' curve	
r	4.0		
w_s	30	Nonlinear small strain behavior in CK_0UC & UE tests on NC RBBC	4
ϕ'_{cs}	33.5	Critical states measured in CK_0UC tests	
ϕ'_m	24	ESP for CK_0UC & CK_0UE at OCR = 1	
m	0.6		
ψ	10		
D_L	1.0	ESP for CK_0UC at OCR = 8	
ρ_α/ρ_c	0.02	Secondary compression data in triaxial tests Reported values of $C_{\alpha\varepsilon}/C_R$	7, 15
β	0.02	Rate-sensitivity of LCC for CRS tests using different strain rates	18, 19
$\dot{\varepsilon}_{ref}$	2×10^{-7}/s	Applied strain rate in triaxial consolidation	4
β_2	6.8	Creep at OC states (inferred from data using SLC clay)	20
β_3	19		

(1) ρ_c characterizes the compressibility of normally consolidated (NC) clay, and corresponds to the slope of the limiting compression curve (LCC) plotted in logarithmic void ratio-logarithmic effective stress, log$e$-logσ'_v, space (this assumes K_{0NC} is approximately constant for NC states). Figure 1 plots typical LCC curves for CRS tests and K_0-consolidation phase of triaxial tests on RBBC,[7] from which a linearized relation with the slope $\rho_c = 0.180$ is determined (this is close to the prior value selected 0.178 for MIT-S1[3]).

(2) The lateral pressure coefficient, K_{0NC}, and the Poisson's ratio, ν', can be derived from the K_0-consolidation and 1D unloading/swelling curves in Figure 2. The lateral pressure coefficient and Poisson's ratio for RBBC both evolve with the unloading stress ratio (σ'_h/σ'_p vs σ'_v/σ'_p).[7] The current model uses $K_{0NC} = 0.49$ (typical K_{0NC} for RBBC between 0.47-0.58[4,7,21]), and $\nu' = 0.263$ ($2G/K = 3(1-2\nu')/(1+\nu') = 1.13$).

(3) C_b controls the small strain shear stiffness, and can be estimated from the normalized shear stiffness, G_n:

$$C_b \approx \frac{2}{3} G_n \frac{(1+\upsilon')}{(1-2\upsilon')} \text{ with } G_n = n \frac{(G_{\text{sec}}/p_{atm})}{(\sigma'/p_{atm})^{1/3}}, \tag{1}$$

where n = porosity, p_{atm} = atmosphere pressure (≈ 100 kPa) and G_{sec} = secant shear modulus. Figure 3 plots the evolution of normalized shear stiffness G_n for a series of shear tests on RBBC,[5] from which an averaged value for $C_b = 473$ is obtained for a small strain range 10^{-4}% to 10^{-3}% (close to 450, the value selected previously for MIT-S1[3]).

(4) D and r are determined by fitting the 1D swelling stress-strain response (where the incremental volumetric strain in unloading is plotted against $\log(\sigma'_v/\sigma'_p)$). Figure 4 illustrates the fitting process, in which $D = 0.03$ represents the swelling curve for OCR > 2, while $r = 4$ defines conditions at small OCR < 2.

(5) w_s controls the nonlinearity of the small-strain shear behavior, and is determined from a parametric study to fit the deviator stress versus strain curves measured in CK_0UC and CK_0UE tests on RBBC at OCR = 1.[4] Figure 5 compares computed and measured deviator stress, q/σ'_{vc} [$= (\sigma'_v - \sigma'_h)/\sigma'_{vc}$], versus axial strain, ε_a, response for tests performed at a standard shear strain rate, $\dot{\varepsilon}_a = 0.5\%$. Here the parameter selection involves some judgment. We selected $w_s = 30$ to match the observed strain to peak shear resistance, ε_a, peak ≈ 0.2% in the CK_0UC test, and to represent reasonably the postpeak response to large levels of shear strain ($|\varepsilon_a| = 10\%$) in compression and extension modes.

(6) ϕ'_{cs} is the critical state friction angle under triaxial shear conditions. Figure 6 plots the typical data of stress path (ESP) for CK_0UC and CK_0UE tests on RBBC,[4] from which $\phi'_{cs} = 33.5°$ is estimated at large shear strain levels.

(7) The parameters ϕ'_m and m control the shape of the loading/reference surface, while ψ controls the rotation rate of the reference surface during kinematic hardening. These three parameters need to be determined through a parametric study to fit CK_0UC and CK_0UE data for RBBC at OCR = 1 (at a standard strain rate, $\dot{\varepsilon}_a = 0.5\%$/h). Figures 6(A) and (B)

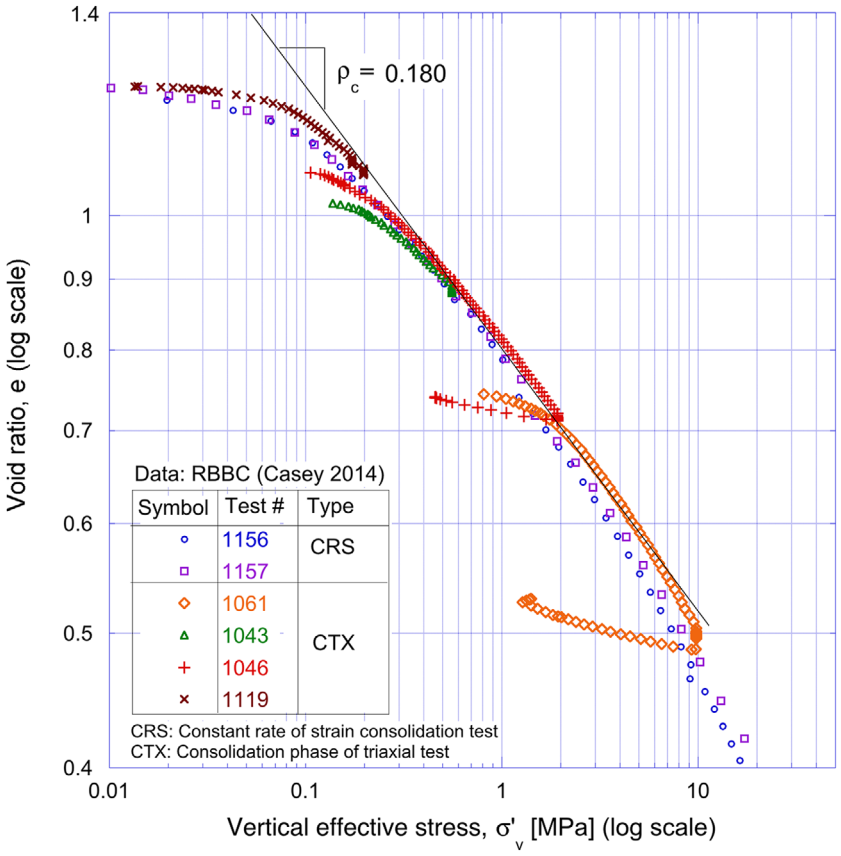

FIGURE 1 Determination of MIT-SR compressibility parameter ρ_c with K_0 consolidation data of RBBC from LCC curves for CRS and triaxial test

illustrate the influence of ϕ'_m and m on the predicted effective stress paths (ESPs) for undrained triaxial compression and extension tests, respectively. The following observations can be made: (i) increasing m leads to a minor decrease in undrained strengths and increased postpeak softening in compression tests; (ii) parameter m has more influence on the behavior of extension tests in terms of the shape of ESPs and undrained strengths; (iii) increasing ϕ'_m results in similar influence on ESPs and associated s_u for compression and extension tests.

The parameter, ψ, controls the rotation rate of the reference surface due to kinematic hardening, and is important for predictions that entail significant evolution of anisotropy. Figures 7(A) and (B) compare the predicted ESPs and stress-strain curves for CK_0UC and CK_0UE tests at OCR = 1 using different values of ψ, respectively. The result shows that ψ has negligible influence on CK_0UC behavior, but more pronounced effects on the CK_0UE behavior, especially over the axial strain range of 5-20%. Therefore, the value of ψ can be determined by fitting the measurements of CK_0UE tests. Figure 8 compares the computed and measured ESPs for selected values of ϕ'_m, m, and ψ. The proposed formulation with $\phi'_m = 24°$ and $m = 0.6$ captures the peak strength and the postpeak softening behavior under CK_0UC conditions, while the use of $\psi = 10$ achieves a reasonable match to the measured CK_0UE behavior.

(8) D_L controls the dilation behavior and is determined by fitting the CK_0UC shear test on RBBC at an OC state. Figure 8 shows that the proposed model with $D_L = 1.0$ provides a good representation of the measured ESP and undrained strength, s_u, for RBBC at OCR = 8.

(9) The rate sensitivity parameter, β, controls the rate-dependency of the limiting compression curves (LCCs) measured in CRS tests. Figure 9(A) plots the LCCs from a series of CRS tests performed on RBBC at strain rates in the range, $\dot{\varepsilon}_a$, = 0.07%/h to 12.7%/h.[18,19] There is a general trend of increasing vertical effective stress with strain rate, and the increment (spacing between two curves) appears to be more pronounced at higher void ratio levels. Figure 9(B) plots the changes in effective stress σ'_v versus the axial strain rates $\dot{\varepsilon}_a$ for a set of void ratios extracted from these data. The results show linearized $\log\sigma'_v$ - $\log\dot{\varepsilon}_a$ relations, where the slope corresponds to $\beta = 0.031$ to 0.012. The average $\beta = 0.020$ is selected for the remaining analyses.

(10) The parameter ρ_α can be interpreted from the creep behavior of RBBC. Figure 10(A) plots the change in void ratio

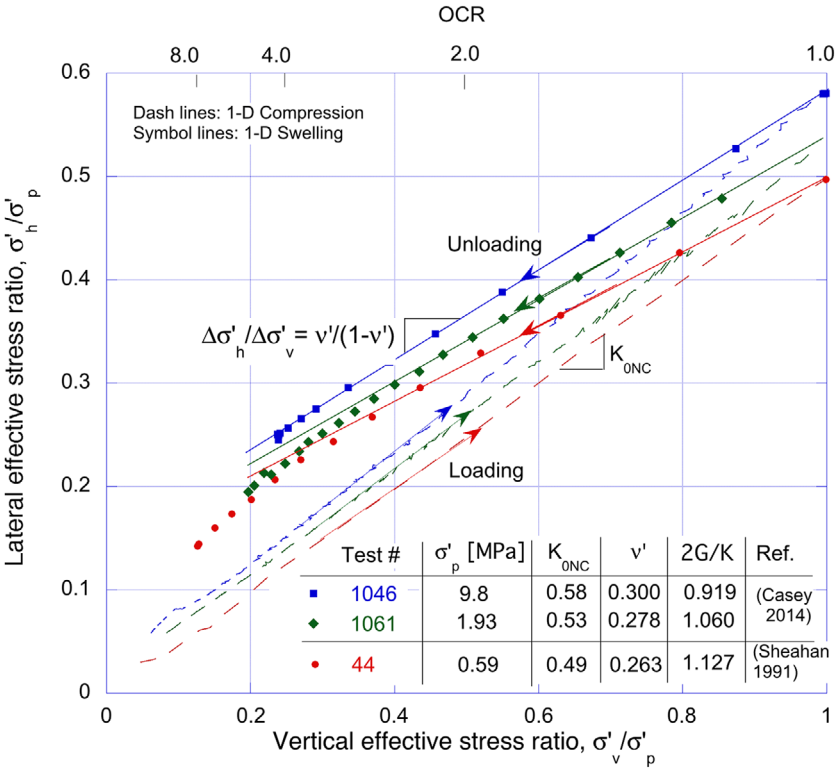

FIGURE 2 Determination of Poisson's ratio ν or parameter $2G/K$ from 1D swelling effective stress path in σ'_h-σ'_v space

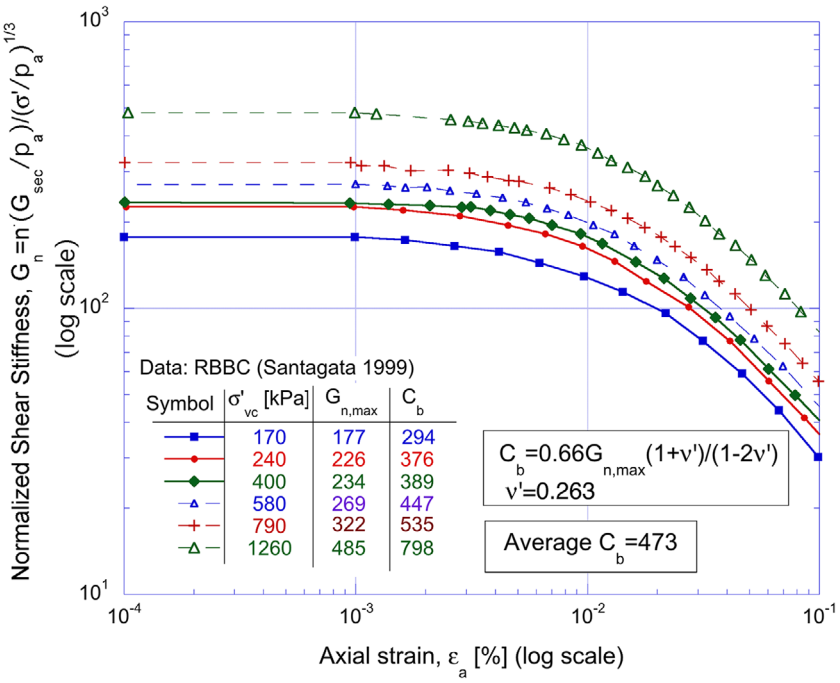

FIGURE 3 Determination of parameter C_b from measurements of small strain shear stiffness in K_0-consolidated triaxial shear tests

with axial strain rate for the creep behavior after primary consolidation under triaxial conditions.[7] The results can be linearized in the log$e$ - log$\dot{\varepsilon}_a$ space, with ρ_α corresponding to the gradient. Figure 10(B) plots a set of the interpreted values of ρ_α versus the compressibility of the NC clay, ρ_c, from a series of triaxial consolidation tests on RBBC.[7] The ratio of ρ_α/ρ_c is generally bounded in a narrow band of $\rho_\alpha/\rho_c = 0.02$ to 0.029, which closely corresponds to the reported range of secondary compression index over compression ratio, $C_{\alpha\varepsilon}/C_R = 0.023 \pm 0.006$ for RBBC.[15] The ratio of $\rho_\alpha/\rho_c = 0.02$ is selected, which coincides with the selected rate-sensitivity, $\beta = 0.02$ for RBBC.

(11) The reference strain rate $\dot{\varepsilon}_{ref}$ is selected as the standard strain rate used in consolidation of RBBC triaxial specimens, $\dot{\varepsilon}_{ref} = 0.1\%/\text{h}$ ($\approx 2 \times 10^{-7}$/s), as shown in Figure 9(B).

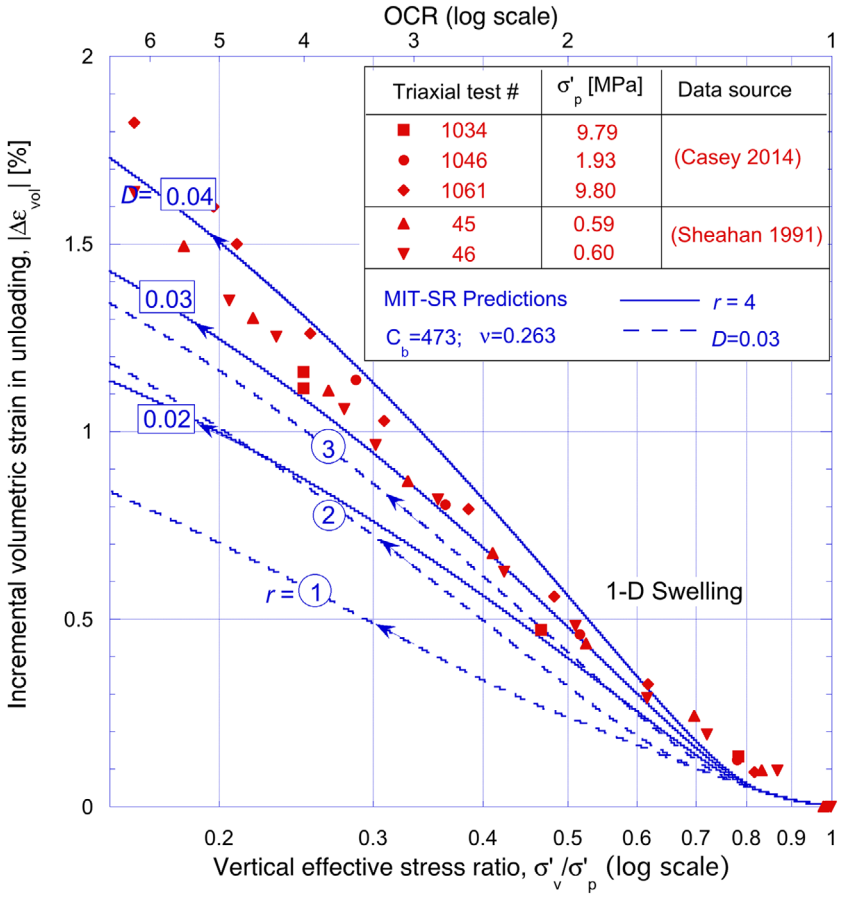

FIGURE 4 Determination of parameters D and r from the data during 1D unloading/reloading

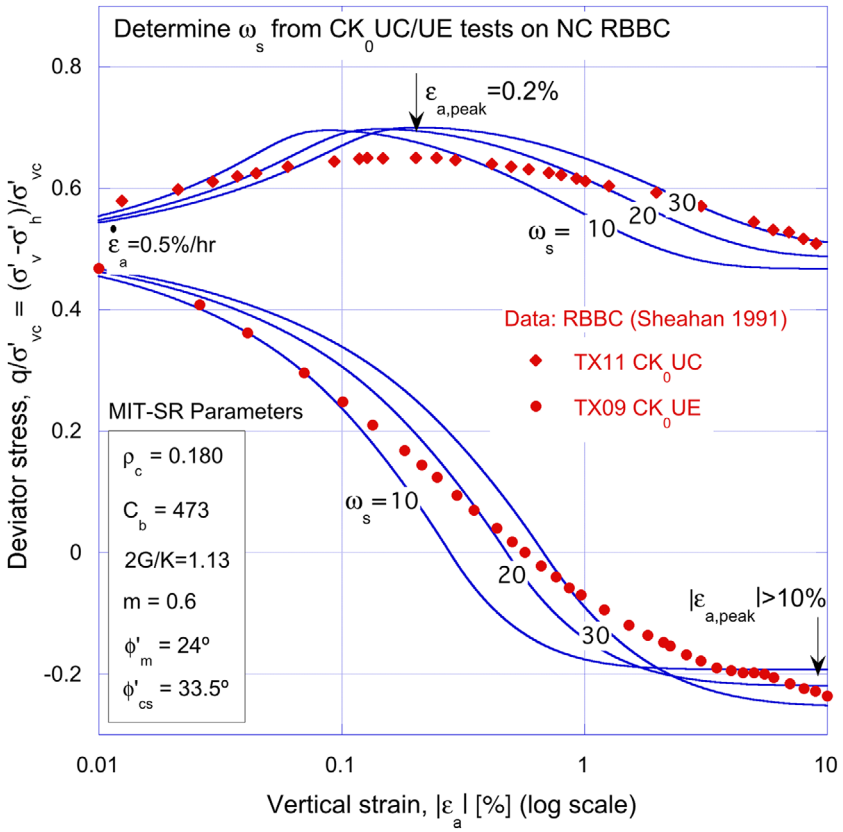

FIGURE 5 Determination of parameter w_s from K0-consolidated triaxial compression and extension tests on RBBC

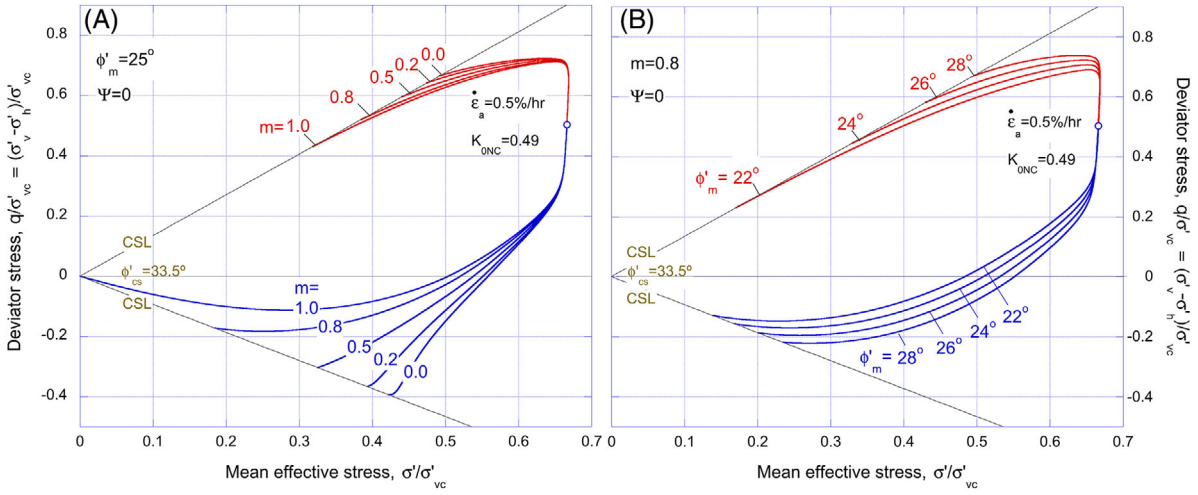

FIGURE 6 Influence of parameters (A) m and (B) ϕ'_m on the predicted ESPs for CK_0UC and CK_0UE tests on normally consolidated clay

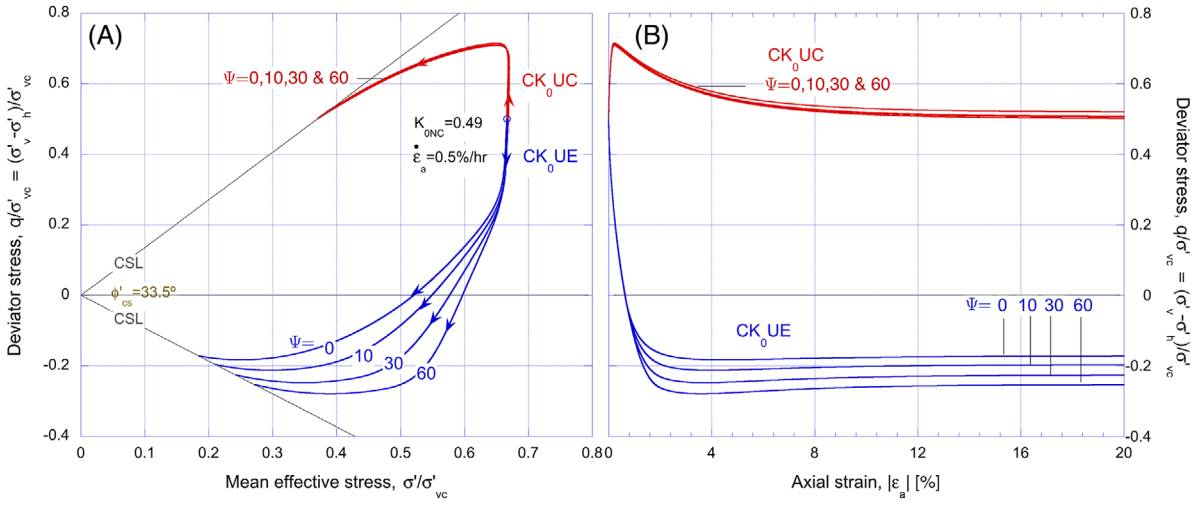

FIGURE 7 Influence of kinematic hardening parameter ψ on the prediction of CK_0UC and CK_0UE tests; (A) effective stress paths and (B) deviator stress-strain curves

(12) Parameters β_2 and β_3 characterize the creep behavior at overconsolidated (OC) states. As illustrated in the companion paper,[1] β_2 controls the variation in the rate-dependency due to stress-history effect, while β_3 governs the decrease in creep strain rate as clay swells upon unloading. In principle, the two parameters can be determined by fitting the measured creep behavior for clay after being unloaded in 1D oedometer tests. However, direct determination of β_2 and β_3 for RBBC is limited by the lack of creep data at OC states. This study uses values $\beta_2 = 6.8$ and $\beta_3 = 19$, which were interpreted from the creep behavior of overconsolidated Salt-Lake-City (SLC) clay ($w_L = 43.5\%$ and $I_P = 21.3\%$,[20]), which has very similar index properties to RBBC (Table 1). The interpretation of SLC data is depicted in the companion paper (figure 5 in Ref. 1) and also presented in Refs. (22, 23). Further data are needed to verify the selected values of β_2 and β_3 for RBBC.

3 | VALIDATION ON RESEDIMENTED BOSTON BLUE CLAY

This section validates the MIT-SR model predictions with the measurements for various undrained shear behavior of RBBC, including[4,14,15,16]

(1) Undrained triaxial compression (CK_0UC) and extension (CK_0UE) behavior at different OCRs

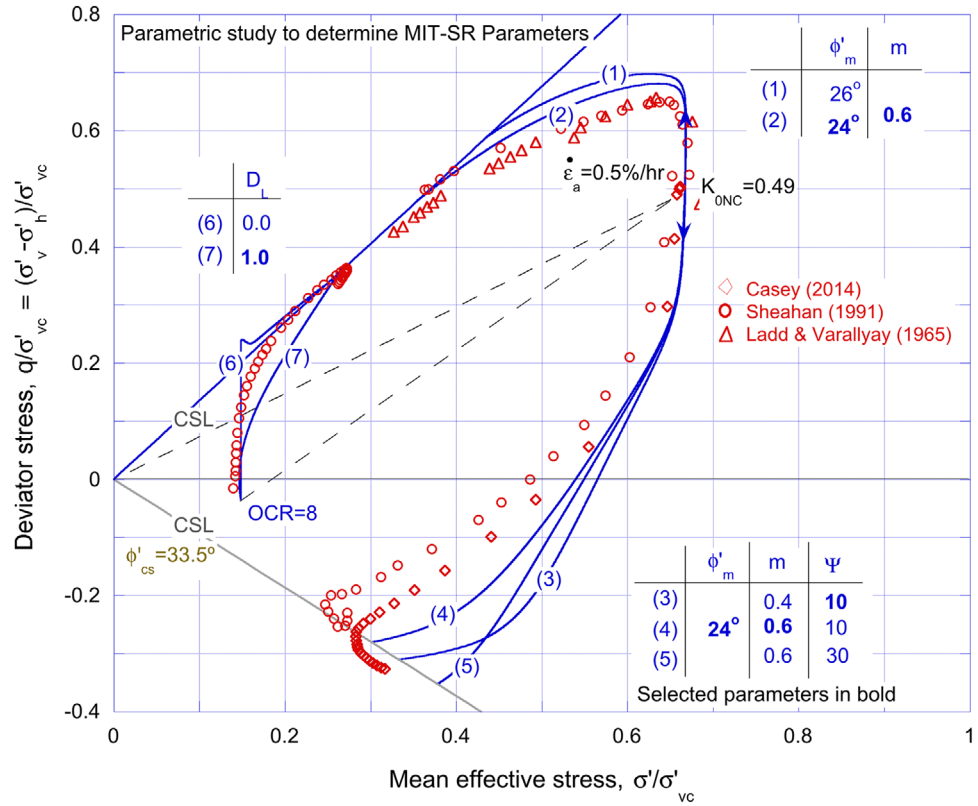

FIGURE 8 Determination of parameters ϕ'_c, m, ϕ'_m, ψ, and D_L from K_0-consolidated triaxial compression and extension tests on normally consolidated RBBC

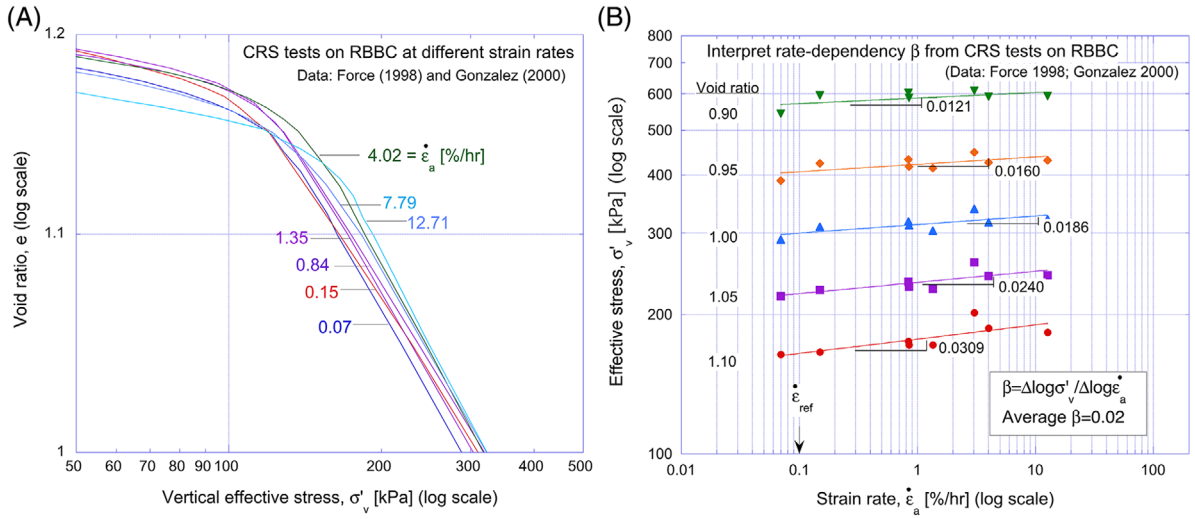

FIGURE 9 Determination of rate-sensitivity parameter β from CRS tests on RBBC at different strain rates (A) LCCs for CRS tests at different strain rates and (B) interpretations of rate-dependency at various void ratios

(2) Strain rate effects on triaxial compression and extension tests, and the stress history influence on the rate-dependency
(3) Undrained relaxation behavior in triaxial shear test
(4) Undrained Direct Simple Shear (CK_0DSS) behavior at different OCRs
(5) Strain rate effects on undrained direct simple shear tests

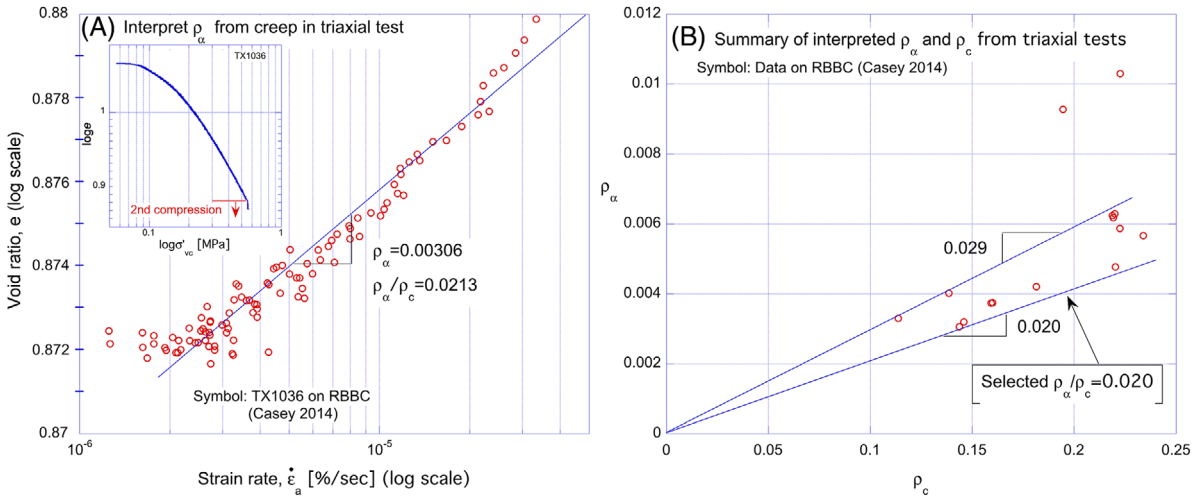

FIGURE 10 Interpretation of (A) parameter ρ_α from the creep data in triaxial tests and (B) interpretation of ratio ρ_α / ρ_c

The MIT-SR model is implemented in a simulator to predict elemental-level constitutive response for the considered tests. The implementation is based on the *Modified Euler* integration scheme,[24] which performs two consecutive explicit integration steps and uses their results to guide the integration accuracy and adjust the time-step size. The companion paper presents the flow charts for this integration algorithm.

The predictions use the calibrated material parameters for RBBC in Table 2 and assume the initial state variables that reflect the stress history associated with sample preparation via resedimentation: In the original experiments, the clay samples were resedimented from slurry and incrementally loaded to the desired effective stress level in a consolidometer. This resedimentation procedure minimizes the variations in void ratio between samples and provides a well-controlled stress history.[6,7,10,11] The consolidated samples were then extruded from consolidometer, trimmed to the desired dimension, and set up in the triaxial or direct simple shear apparatus.

All the simulations of lab tests in this paper proceed from an initial OC effective stress state with OCR = 4, $K_0 = 1$ ($\sigma'_v/p_{atm} = 0.25$) and $e_0 = 1.10$ (consistent with standard triaxial test procedures[4]). The initial size of reference surface, α_0, is set to represent the preconsolidation stress level due to resedimentation, and the orientation of reference surface, $\boldsymbol{b_0}$, is set on K_{0NC} axis. As suggested in the companion paper, the hysteretic parameters assume default values $\boldsymbol{\eta}^{h0} = \boldsymbol{\eta}^0$, $\sigma^{h0} = \sigma'_0$ for OC states. The internal strain rate, $R_{a0} = 0$ to render a negligible creep rate at the initial OC state.

Modeling of the preshear consolidation and creep phases in a triaxial shear test is critical for the MIT-SR to predict the initial creep rate for the succeeding shearing phase. Hence, the present simulations follow closely the sequence of the experiment phases used in the original laboratory tests: (1) the soil specimen is consolidated under K_0 condition to a desired NC stress level (much higher than preconsolidation pressure based on SHANSEP procedure[17]) with a constant axial strain rate, $\dot{\varepsilon}_a = 0.1\sim0.15\%/h$ and (2) creep is allowed to occur under drained conditions for 24 hours; (3) for tests in the OC range, the specimen is unloaded to a desired OCR at $\dot{\varepsilon}_a = 0.1\%/h$ and is kept fixed for 24 hours; and (4) the specimen is then sheared at specified strain rates under undrained conditions.

3.1 | Triaxial shear at different OCRs

The MIT-SR predictions are compared to the measurements for undrained triaxial compression (CK_0UC) and extension (CK_0UE) tests on RBBC,[4] sheared at a standard strain rate $\dot{\varepsilon}_a = 0.5\%/h$ for four OCRs (= 1.0, 2.0, 4.0, and 8.0). Figures 11(A) and 11(B) plot the effective stress paths, and deviator stress-axial strain curves, respectively, where the stresses are normalized by the (conventional) vertical preconsolidation stress, σ'_p.

In general, the calibrated MIT-SR model provides a reasonable match to the reported measured effective stress paths and stress-strain behavior in triaxial compression and extension shear modes at all OCRs. At the beginning of shearing, the model predicts increasing stress with negligible change in mean effective stress (Figure 11A). This behavior is attributed to the considerably reduced viscoplastic strain rate (associated with the preshear creep phase) and is consistent with the measurements. The predictions for CK_0UC test reproduce the contractive behavior of ESP at

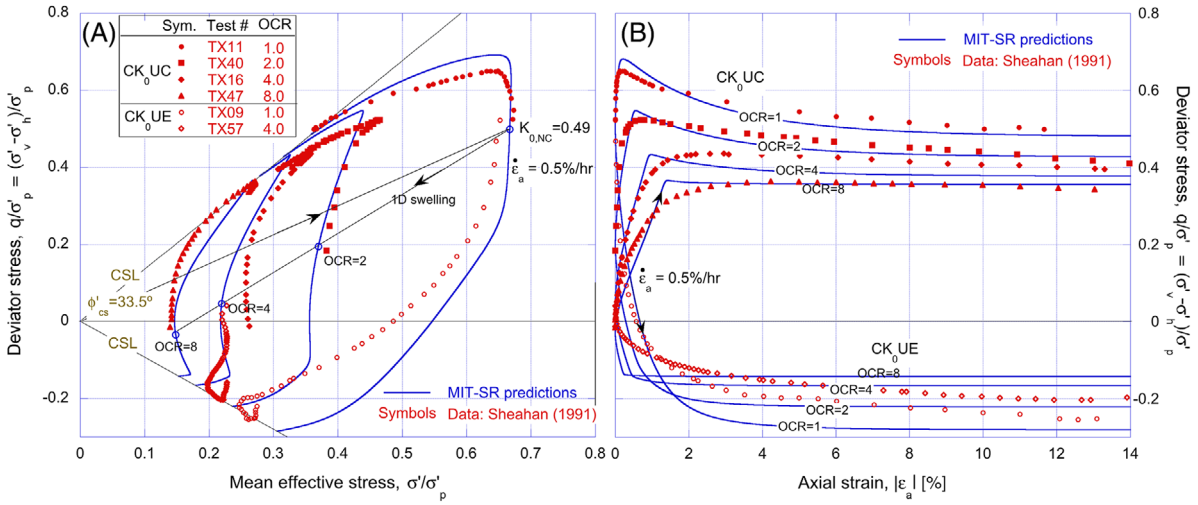

FIGURE 11 Comparison between predictions and measured (A) effective stress paths and (B) deviator stress-axial strain curve for CK_0UC and CK_0UE tests on RBBC for various OCRs

OCR = 1 and the dilative behavior that increases with OCR, and match the measured undrained shear strengths and the postpeak softening behavior. The predictions of CK_0UE test are also in good agreement with the measurements for the reported two OCRs. The following sections evaluate in-depth the strain rate effects of the triaxial shear behavior of RBBC.

3.2 | Strain rate effect on triaxial shear behavior

The MIT-SR model is used to simulate a comprehensive set of triaxial compression (CK_0UC) tests on RBBC, sheared at OCRs = 1, 2, 4, and 8, using axial strain rates $\dot{\varepsilon}_a$ = 0.05, 0.5, 5, and 50%/h, as reported by Sheahan.[4,14] Figures 12(A) and (B) compare the MIT-SR predictions with measurements of effective stress paths (ESP) and deviator stress-axial strain responses for CK_0UC tests at OCR = 1, while Figures 12(C)-(H) provide the comparisons at OCRs = 2, 4, and 8. Some detailed observations are as follows:

(1) At OCR = 1 and 2, the predicted ESP curves agree very well with the measurements over the full range of axial strain rates (Figures 12A and C). The shear response for the normally consolidated clay (Figure 12A) initially shows increase in deviator stress with minimum change in mean effective stress for all strain rates, while at OCR = 2 (Figure 12C) there is small negative shear-induced pore pressure before peak. The predicted undrained strengths, s_u/σ'_p, increase with strain rates from 0.05 to 50%/h, but the increment is more pronounced for OCR = 1. At OCR = 4 and 8, Figures 12(E) and (G) show more pronounced dilative behavior in the associated ESPs, and exhibit much smaller rate-dependency for the predicted peak strengths.

(2) Figures 12(B) and (D) show the deviator stress versus axial strain curves at OCR = 1 and 2, which are also in good agreement with the data. The axial strains to the peak shear resistance show negligible changes with strain rates and lie in a narrow range of ε_a = 0.2~0.25% and 0.6~0.8% for OCR = 1 and 2 (Figures 12B, D), respectively. Noticeable rate-dependency is observed for the predicted deviator stress at large strain levels, $\varepsilon_a > 10\%$, consistent with the data. Figures 12(F) and (H) show that the predicted peak strengths for OCR = 4 and 8 occur at a larger strain levels, and the postpeak curves show less softening (or even develop strain hardening at high strain rate), when compared to the above cases with OCR = 1 and 2. The predicted deviator stress-strain curves for OCR = 4 and 8 also exhibit noticeable rate-dependency at large strain levels similar to the measured data.

(3) As noted in the companion paper,[1] under triaxial compression the MIT-SR prediction of shear behavior at large strain level corresponds to the steady state of the internal strain rate, R_a. The rate-dependency at large axial strain levels is mainly controlled by the rate-sensitivity parameter, β. Using β = 0.02 leads to modest rate-dependency of shear resistance at large strain levels, which is generally consistent with the measured data.

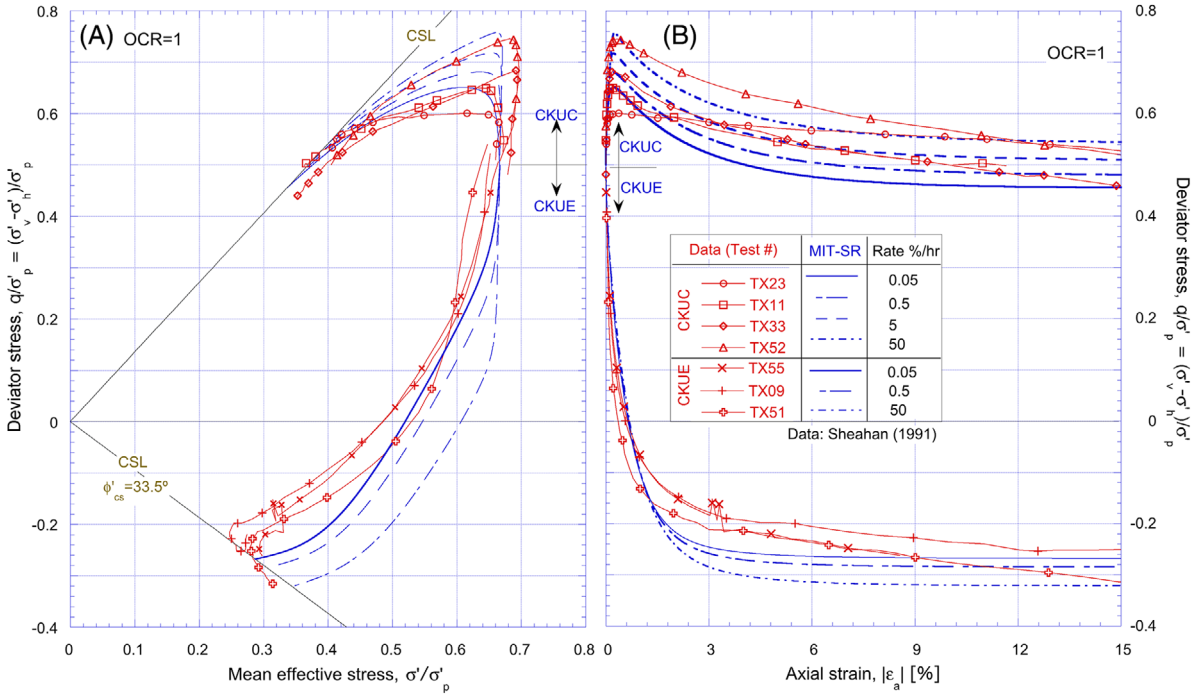

FIGURE 12 Strain rate effects on triaxial compression and extension test on RBBC for OCR = 1: (A) effective stress paths and (B) deviator stress-strain curves. Strain rate effects on triaxial compression tests of RBBC: (C, E, G) stress paths; and (D, F, H) deviator stress-strain curves for OCR = 2, 4, and 8, respectively

Figure 13 summarizes the measured undrained shear strengths, s_u/σ'_p, for RBBC at four OCRs = 1.0, 2.0, 4.0, and 8.0, plotted against the applied strain rates, $\dot{\varepsilon}_a$ (= 0.05, 0.5, 5.0 and 50%/h) in a double logarithmic space. The data leads to a key implication that the rate-dependency for the normalized undrained shear strength, s_u/σ'_p, of the RBBC appears to decrease with OCRs.[4] Preexisting time-dependent soil models are not able to represent this influence of stress history on rate-dependency, as many of them presume a unique stress-strain-strain rate relationship,[25] and thus can only represent constant rate-dependency for s_u/σ'_p over different OCRs.

Figure 13 plots the MIT-SR predictions of s_u/σ'_p for all OCRs, which show linearized increase in s_u/σ'_p with strain rates in the double logarithmic space, with the slope indicating the rate-dependency. The result for the NC state shows a maximum rate-dependency of 0.022 for s_u/σ'_p (ie, approximately 5% increase in s_u per log cycle of $\dot{\varepsilon}_a$), whereas the predicted rate-dependency for s_u/σ'_p dramatically decreases with OCRs. These trends are generally comparable with the measurements. As noted in the companion paper,[1] the strain rate effects of undrained peak strengths under triaxial compression at NC state is primarily dominated by the transient behavior of internal strain rate, R_a, but this transient characteristic at peak strengths appears to reduce with OCRs, and results in negligible rate-dependent s_u/σ'_p at OCR $\geq$ 2.

The MIT-SR model predictions are also compared to the measured strain rate effects for CK_0UE tests on RBBC, sheared at OCR = 1.0 using a set of strain rates $\dot{\varepsilon}_a$ = 0.05, 0.5, and 50%/h.[4] Figures 12(A) and (B) plot the ESPs and deviator stress-axial strain responses for these extension tests, respectively. The MIT-SR model represents accurately the increase in the large strain shear resistance with strain rate and the effects of strain rate on the development of shear-induced pore pressures (ESPs).

Figures 14(A) and (B) present further investigations to reveal the influence of β on predictions of CK_0UC tests with step-changed strain rates (for $\beta = \rho_\alpha/\rho_c = 0.02$). The plots show computed simulations of CK0UC tests subject to a series of stepped changes in axial strain rate, $\dot{\varepsilon}_a$ (= 5.0, 0.5, and 0.05%/h). The deviator stress-strain curve exhibits features that are similar to isotache models (Figure 14B; ie, the postpeak curve is displaced in parallel from one isotache to another upon step-change in $\dot{\varepsilon}_a$). On the other hand, the effective stress path (Figure 14A) clearly overshoots the reference (ie, constant strain rate shear) paths with each step-change in $\dot{\varepsilon}_a$. This becomes more pronounced near critical state conditions and reflects transient effects in the internal strain rate, R_a, upon step-changes in $\dot{\varepsilon}_a$ in undrained shearing.

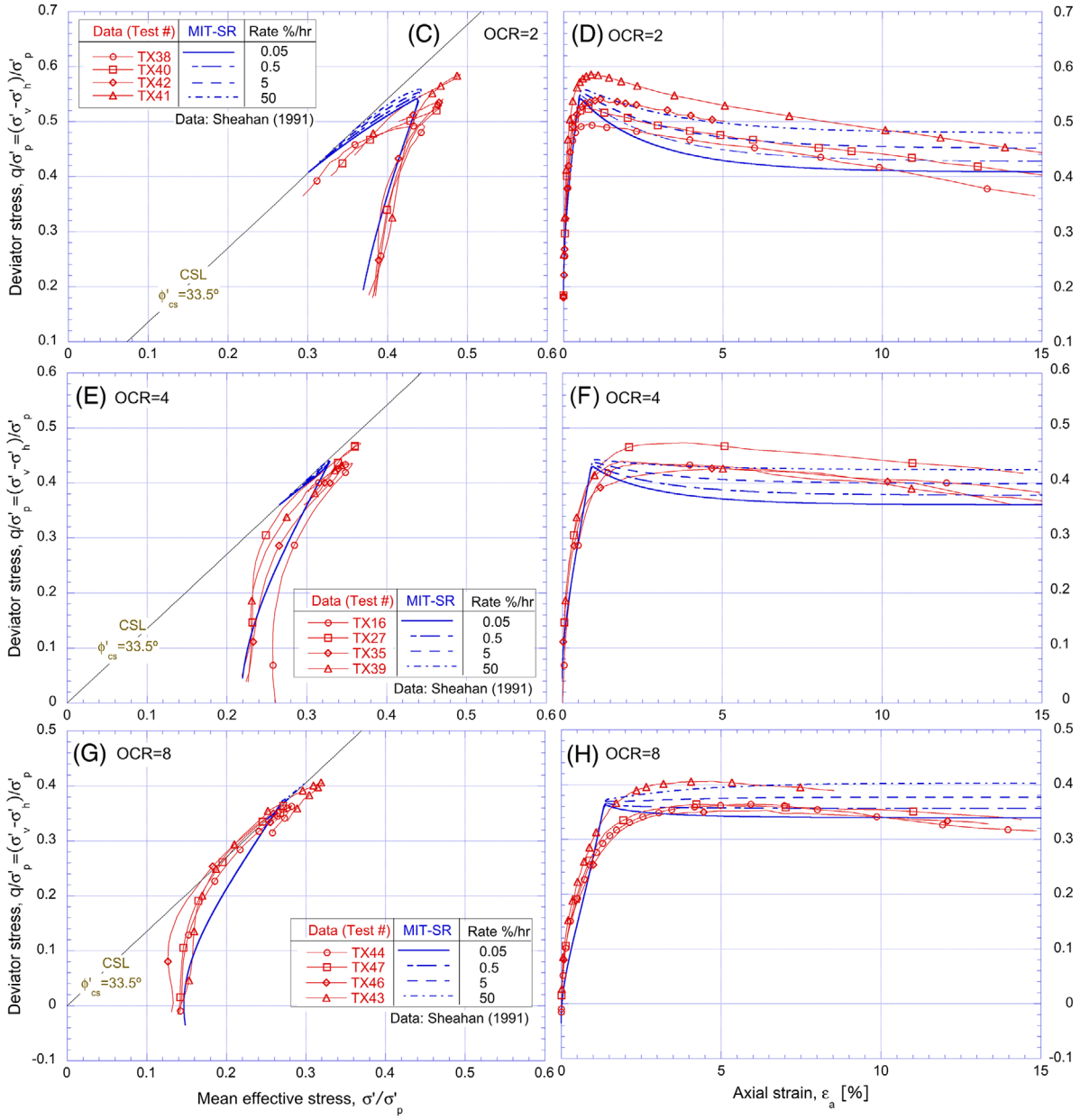

FIGURE 12 Continued

3.3 | Undrained relaxation behavior in CK_0UC tests

The undrained relaxation behavior for RBBC was evaluated in a special type of CK_0UC test for normally consolidated samples.[4] The test procedure consisted of an undrained shearing phase at an axial strain rate of 50%/h, that is interrupted at a set of selected strain levels (eg, ε_a = 0.1%, 1%, 10%, and 15%), to allow relaxation. During each relaxation phase, the specimen is restricted from deformation under undrained conditions with constant cell pressure. During relaxation the deviator stress decreases with time for 0.1~3 days until there is no detectable change in stress over a period of 4~8 hours. Figures 15(A) and (C) show the measured effective stress paths and the change in the deviator stress versus time curve for these relaxation tests, respectively.

The MIT-SR simulations use the calibrated material parameters and closely follow the experiment procedure for the shearing process and the sequence of relaxation phases. Figures 15(B) and (D) show that the MIT-SR model achieves reasonable predictions of these multiphase relaxation experiments from different states of undrained shear (initial axial strain levels) but tends to underestimate the measured changes in deviator stress.

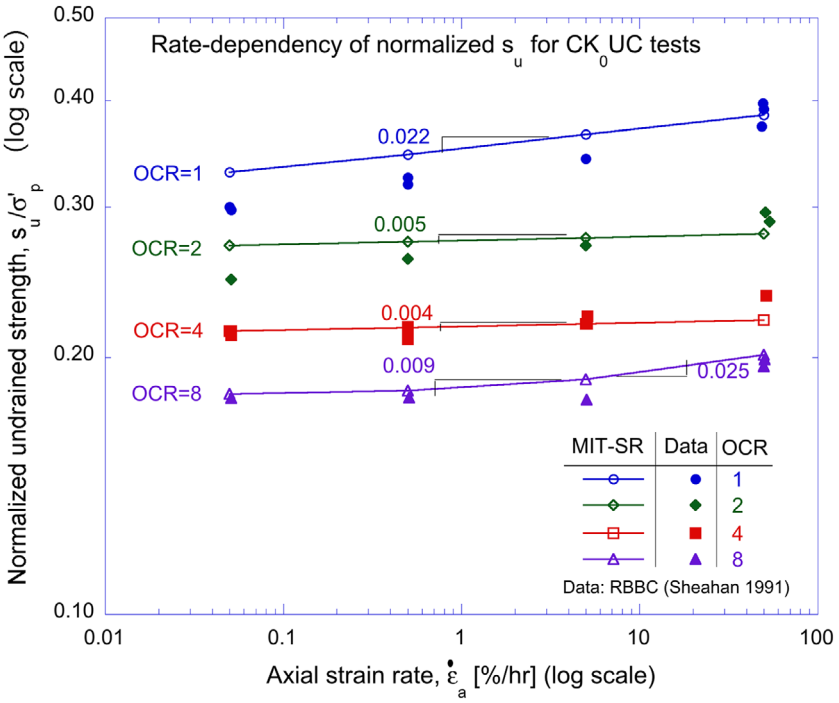

FIGURE 13 Summary of changes in rate-dependency of normalized s_u/σ'_p for CK_0UC with OCRs

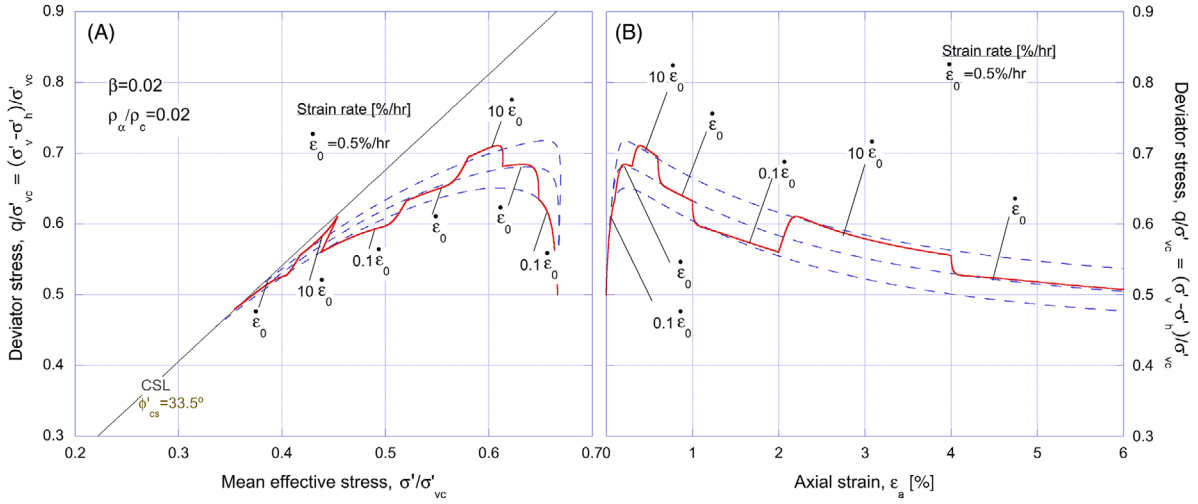

FIGURE 14 MIT-SR model prediction of CK_0UC tests for RBBC with step changed strain rates (A) effective stress paths; (B) deviator stress-strain curves

3.4 | Undrained direct simple shear tests

This section benchmarks the MIT-SR predictions with the K_0-consolidated direct simple shear (CK_0UDSS) test on RBBC at four OCRs (= 1.0, 2.0, 3.25, and 8.0).[15] The reference tests were conducted in a Geonor DSS apparatus[26] and consist of the following phases: (1) K_0-consolidation under 24-hour interval, incrementally loaded (IL) oedometer conditions to a specified effective stress level within a wire-reinforced membrane; (2) for OC states, the specimens are unloaded using 24-hour interval IL conditions to the specified OCR; (3) shearing at a controlled strain rate (eg, $\dot{\gamma} = 5\%/h$) on the top surface of the specimen, while maintaining a constant volume (through feedback control of total vertical stress) to emulate undrained shear conditions. The MIT-SR simulations generally follow the reported experiment procedure. It is difficult to use the elemental level simulation to reproduce the actual strain rate history for the 24hr-interval IL consolidation in these DSS tests. Instead, the K_0-consolidation phases are simulated with CRS consolidation at an equivalent strain rate,

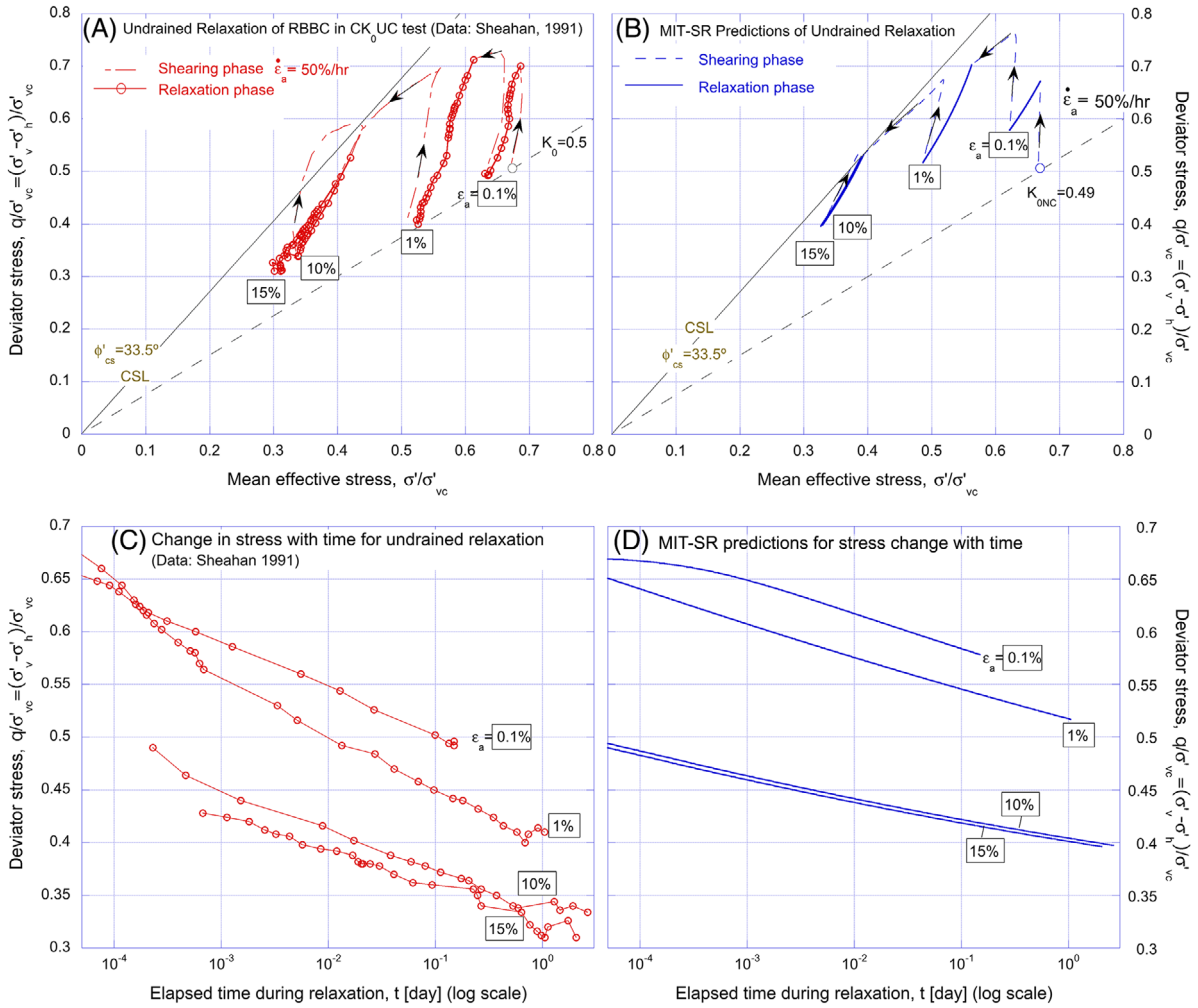

FIGURE 15 Effective stress paths for the undrained relaxation behavior of RBBC (A) measurements and (B) MIT-SR predictions. Change in stress with time for the undrained relaxation behavior of RBBC: (C) measurements and (D) MIT-SR predictions

which corresponds to the measured strain rate at the end of 24-hour interval ($\dot{\varepsilon}_a \approx 1 \times 10^{-7}$/s). The predicted DSS shear behavior is compared to the reported data.

Figures 16(A) and (B) plot the shear stress-vertical effective stress, $\tau/\sigma'_p - \sigma'_v/\sigma'_p$ paths and the shear stress versus strain, τ/σ'_p-γ curves, respectively. The computed effective stress paths are generally in good agreement with the measurements at all four OCRs as shown in Figure 16(A). The prediction for the normally consolidated specimen shows contractive behavior and matches the measured peak undrained strengths. At OCR = 2.0 and 3.25, the predicted ESPs initially show a dilation trend followed by postpeak softening, which are in good agreement with the measured behavior, although the predicted strengths are slightly lower than the measurements. The predicted effective stress path at OCR = 8 shows dilation trend up to the peaks and the predicted peak strength is slightly higher than experimental results. The predicted stress obliquities, show average value of $\tan^{-1}(\tau_h/\sigma_v) = 27.2°$ at large strains, which is close to the reported value, 30°.[15] Figure 16(B) shows that the predictions generally agree with the measurements for the shear stress-strain curves, although the predicted curves exhibit stiffer behavior and results in smaller strain levels to the peaks than the measured data especially at higher OCR.

3.5 | Strain rate effects in undrained direct simple shear

Shear strain rate effects were also measured in DSS tests,[16] in which the specimen was sheared at OCR = 4.0 using "slow" rates ($\dot{\gamma}$ = 0.71 and 4.6%/h; using the Geonor device) and "fast" strain rates ($\dot{\gamma}$ = 6400 and 12,000%/h; using an MTS device).

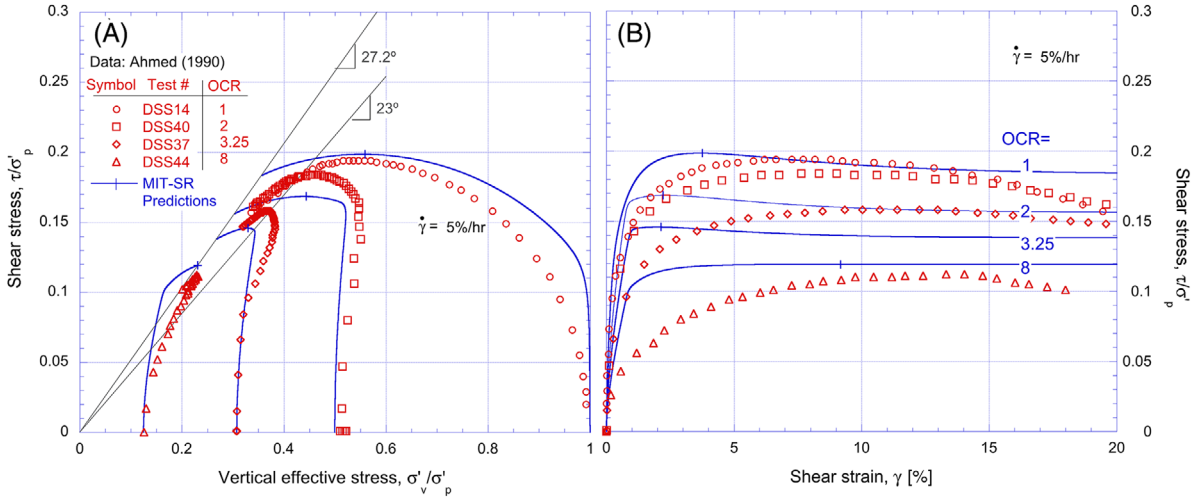

FIGURE 16 Comparisons between MIT-SR prediction and the measured direct simple shear behavior of RBBC at various OCRs: (A) effective stress paths and (B) shear stress-strain curves

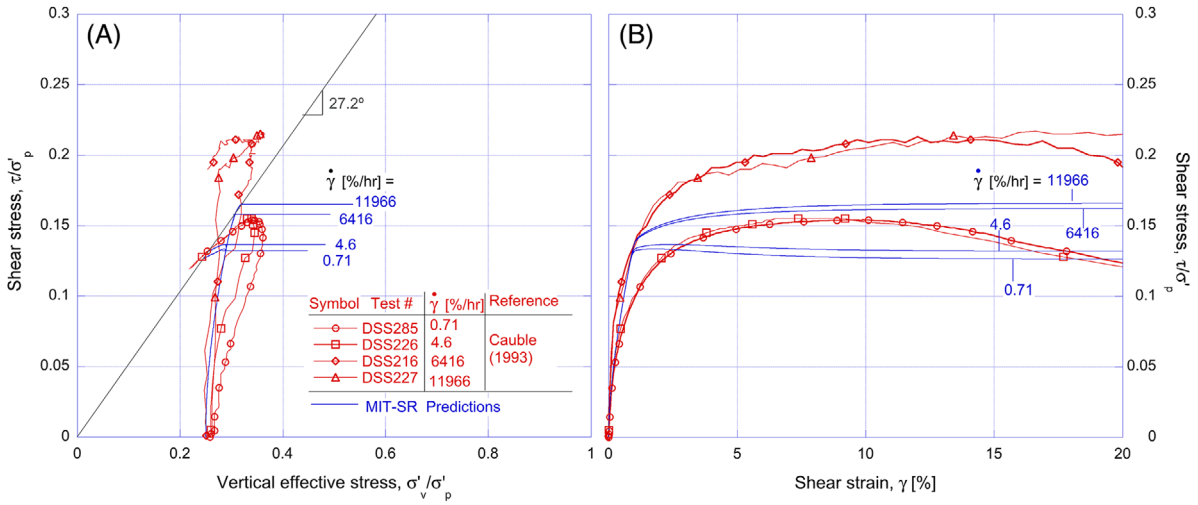

FIGURE 17 Strain rate effects on DSS test of RBBC at OCR = 4: (A) effective stress paths and (B) shear stressstrain curves

Figures 17(A) and (B) compare the MIT-SR predictions with the laboratory measured effective stress paths and shear stress-strain curves for these DSS tests, respectively. For slow shearing, the predicted stress paths show dilation characteristics as shear stress increases to the peak followed by postpeak softening behavior, qualitatively consistent with the data; while the predictions for fast shearing show continuous increase in stress with traces of softening until large strain levels, also similar to the laboratory observations. The measured data show pronounced strain rate effects when comparing the "fast" tests with the "slow" ones, with 33% increase in shear stress, τ, as strain rate $\dot{\gamma}$ increases from 4.6 to 6416%/h. The MIT-SR predictions generally capture the trend of increasing shear stress with strain rates, although the predicted increments in stresses with strain rate appear smaller than the measured data.

4 | CONCLUSIONS

This paper details the calibration of the proposed MIT-SR formulation using a limited number of standard experiments on Resedimented Boston Blue Clay (RBBC). Most of the proposed parameters can be determined by using similar procedures to those for calibrating MIT-S1 model[3]; the five parameters pertinent to the rate-dependent behavior can be interpreted from the consolidation data in CRS tests using different strain rates and the creep data after consolidation.

The performance of the calibrated model has been validated with a series of experiment measurements and the key observations are summarized as follows:

(1) Comparisons with the measurements show good agreement for CK_0UC and CK_0UE tests at OCRs from 1 to 8. The MIT-SR simulations emulate the actual experiment procedure and accurately represent the effective stress-strain-strength characteristics of K_0-consolidated specimens under triaxial shear.
(2) The proposed model has captured strain rate effects on CK_0UC tests at OCR = 1, and well represented the rate-dependent undrained peak shear strength, s_u, and the effective stress-strain characteristics at strain rates $\dot{\varepsilon}_a$ = 0.05, 0.5, 5, and 50%/h.
(3) The MIT-SR model has shown strong capabilities to represent the combined effects of stress history and shear strain rate in CK_0UC tests, capturing the measured trend of decreasing rate-dependency in the normalized undrained strength ratios with OCR.
(4) The MIT-SR predictions for undrained relaxation behavior also achieve reasonable agreement with the measurements, describing the decreasing in deviator stress with time during relaxation.
(5) The MIT-SR model also shows great potential in describing effects of stress history and strain rate for undrained DSS tests, using a more limited set of available test data.

These validations highlight the predictive capabilities of the proposed MIT-SR model, and provide a sound basis for its practical use in more complex boundary value analyses.

ACKNOWLEDGMENTS

This research was supported in part by Ferrovial-Agroman through the MIT-Ferrovial program and by the MIT-Singapore Alliance for Research and Technology (SMART). The Authors are particularly thankful to Professor Thomas Sheahan (Northeastern University) and Dr. Brendan Casey (formerly MIT, now at MBTA) for generously providing the RBBC data and Mauro G. Sottile (now at SBK, Buenos Aires) who assisted in digitalizing the data for model validation. The Authors are especially grateful to Professor John Germaine (formerly MIT, now at Tufts University) for insightful advice on experimental procedures and soil behavior.

DATA AVAILABILITY STATEMENT

The current research uses existing datasets, which are openly available in the literature as cited in the references section. The authors plan to make the code for the MIT-SR soil model available on GitHub.

ORCID


Yixing Yuan https://orcid.org/0000-0002-3408-0358

REFERENCES

1. Yuan Y, Whittle AJ. Formulation of a new elastoviscoplastic model for time-dependent behavior of clay. *Int J Numer Anal Methods Geomech*. 2020. https://doi.org/10.1002/nag.3173.
2. Pestana JM, Whittle AJ. Formulation of a unified constitutive model for clays and sands. *Int J Numer Anal Methods Geomech*. 1999;23(12):1215-1243.
3. Pestana JM, Whittle AJ, Salvati LA. Evaluation of a constitutive model for clays and sands: part II—clay behavior. *Int J Numer Anal Methods Geomech*. 2002;26(11):1097-1121.
4. Sheahan TC. An experimental study of the time-dependent undrained shear behavior of resedimented clay using automated stress path triaxial equipment. PhD Thesis, Massachusetts Institute of Technology, Cambridge, MA; 1991:952.
5. Santagata M. Factors affecting the initial stiffness and stiffness degradation of cohesive soils. PhD Thesis, Massachusetts Institute of Technology, Cambridge, MA; 1999:336.
6. Abdulhadi NO. An experimental investigation into the stress-dependent mechanical behavior of cohesive soil with application to wellbore instability. PhD Thesis, Massachusetts Institute of Technology, Cambridge, MA; 2009:459.
7. Casey B. *The Consolidation and Strength Behavior of Mechanically Compressed Fine-Grained Sediments*. PhD Thesis, Cambridge, MA: Massachusetts Institute of Technology; 2014:259.
8. Ladd CC, Whittle AJ, Legaspi DE. Stress-deformation behavior of an embankment on Boston Blue Clay. *Vertical and Horizontal Deformations of Foundations and Embankments*. ASCE Geotechnical Special Publication No. 40; 1994:1730-1759.
9. Whittle AJ, Sutabutr T, Germaine JT, Varney A. Prediction and interpretation of pore pressure dissipation for a tapered piezoprobe. *Géotechnique*. 2011;51(7):601-617.

10. Germaine JT. Development of the directional shear cell for measuring cross-anisotropic clay properties. ScD Thesis, Massachusetts Institute of Technology, Cambridge, MA; 1982:569.
11. Seah T. Anisotropy of Resedimented Boston Blue Clay. PhD Thesis, Massachusetts Institute of Technology, Cambridge, MA; 1990:1063.
12. Whittle AJ. Evaluation of a constitutive model for overconsolidated clays. *Géotechnique*. 1992;43(2):289-313.
13. Whittle AJ, DeGroot DJ, Ladd CC, Seah T. Model prediction of anisotropic behavior of Boston Blue Clay. *ASCE, J Geotech Eng*. 1994;120(1):199-224.
14. Sheahan TC, Ladd CC, Germaine JT. Rate-dependent undrained shear behavior of saturated clay. *ASCE, J Geotech Eng*. 1996;122(2):99-108.
15. Ahmed I. Investigation of normalized behavior of resedimented Boston Blue Clay using Geonor Direct simple shear apparatus. SM Thesis, Massachusetts Institute of Technology, Cambridge, MA; 1990:372.
16. Cauble DF. An experimental investigation of the behavior of a model suction caisson in a cohesive soil. PhD Thesis, Massachusetts Institute of Technology, Cambridge, MA; 1997:627.
17. Ladd CC, Foott R. New design procedure for stability of soft clays. *ASCE, J Geotech Eng Div*. 1974;100(GT7):763-786.
18. Force EA. Factors controlling pore pressure generation during K_0-consolidation of laboratory tests. SM Thesis. Massachusetts Institute of Technology, Cambridge, MA; 1998:166.
19. Gonzalez JH. Experimental and theoretical investigation of constant rate of strain consolidation. SM Thesis, Massachusetts Institute of Technology, Cambridge, MA; 2000:294.
20. Ng NSY. Characterization of consolidation and creep properties of Salt Lake City clays. SM Thesis, Massachusetts Institute of Technology, Cambridge, Massachusetts; 1998:426.
21. Ladd CC, Varallyay J. The influence of stress system on the behavior of saturated clays during undrained shear. *Research Report R65-17, Soil Publication No. 117*, Department of Civil Engineering, Massachusetts Institute of Technology, Cambridge, MA; 1965.
22. Yuan Y. *A New Elasto-Viscoplastic Model for Rate-Dependent Behavior of Clays*. PhD Thesis, Cambridge, MA: Massachusetts Institute of Technology; 2016:387.
23. Yuan Y, Whittle AJ, Nash DFT. Model for predicting and controlling creep settlements with surcharge loading. *Proceedings of the 6th International Symposium on Deformation Characteristics of Geomaterials*, Buenos Aires; 2015:931-938
24. Sloan SW. Substepping schemes for the numerical integration of elastoplastic stress-strain relations. *Int J Numer Methods Eng*. 1987;24(5):893-911.
25. Suklje L. The analysis of the consolidation process by the isotaches method. *Proceedings of the 4th International Conference on Soil Mechanics and Foundation Engineering*, London; 1957;1:201-206.
26. Bjerrum L, Landva A. Direct simple shear tests on Norwegian quick clays. *Géotechnique*. 1966;27(1):13-36.

How to cite this article: Yuan Y, Whittle AJ. Calibration and validation of a new elastoviscoplastic soil model. *Int J Numer Anal Methods Geomech*. 2020;1–17. https://doi.org/10.1002/nag.3173